Available online at www.sciencedirect.com
SCIENCE DIRECT®
Journal of Molecular Spectroscopy 231 (2005) 1–14
Journal of MOLECULAR SPECTROSCOPY
www.elsevier.com/locate/jms

60-GHz oxygen band: precise broadening and central frequencies of fine-structure lines, absolute absorption profile at atmospheric pressure, and revision of mixing coefficients

M.Yu. Tretyakov[a,*], M.A. Koshelev[a], V.V. Dorovskikh[a], D.S. Makarov[a], P.W. Rosenkranz[b]

[a] *Institute of Applied Physics of RAS, 46 Uljanova street, 603950 Nizhnii Novgorod, Russia*
[b] *Massachusetts Institute of Technology, Cambridge, MA 02139, USA*

Received 23 September 2004; in revised form 18 November 2004
Available online 20 January 2005

Abstract

The 60-GHz band of $^{16}O_2$ was studied at room temperature and at low (up to 4 Torr) and atmospheric pressures. Precision measurement of central frequencies, self-broadening, and N_2-broadening parameters of fine-structure transitions up to $N = 27$ was performed by use of a spectrometer with radio-acoustic detection (RAD). The measured parameters are compared with GEISA/HITRAN databanks, MPM92, and other known data. An improved set of the oxygen fine-structure spectroscopic constants is obtained. The absorption profile was recorded in the range 45–96 GHz for laboratory air and pure oxygen at atmospheric pressure by use of a resonator spectrometer with noise level of about ± 0.05 dB/km, and used for deducing the first-order line mixing coefficients and for quantitative assessment of second-order mixing effects. A refined set of MPM parameters is derived from the new data and presented here.

Keywords: Oxygen; 60-GHz; Microwaves; Fine-structure transitions; Pressure broadening; Precise measurements; Absolute absorption profile; Mixing coefficients; Millimeter-wave propagation model

1. Introduction

The 60-GHz oxygen absorption band is formed by a series of magnetic-dipole transitions within the $^3\Sigma$ electronic ground state. Due to electronic spin, rotational levels of the oxygen molecule are each split into a spin triplet corresponding to the three possible space orientations of the total electronic spin vector **S**. If **N** is rotational angular momentum, then the resultant angular momentum is $\mathbf{J} = \mathbf{N} + \mathbf{S}$. Due to symmetry reasons only odd N are allowed. Since for the oxygen molecule spin $S = 1$, possible values for total angular momentum quantum number J are $N + 1$, N, $N - 1$. Lines corresponding to transitions within these triplets ($\Delta N = 0$) are also called fine-structure transitions. The selection rule $\Delta J = \pm 1$ leaves only two series of lines: $J' = N$, $J = N + 1$ (usually denoted as $N+$ lines) and $J' = N$, $J = N - 1$ ($N-$ lines). Other transitions with nonzero ΔN appear at submillimeter wavelengths.

Collisional broadening at increased pressures causes the 60-GHz band lines to blend together and at pressures approaching atmospheric and higher the band absorption looks like an unstructured composite feature spreading about ± 10 GHz around 60 GHz, and one isolated line at 118.75 GHz. Because of the line mixing effect (overlap interference), the resulting intensity of the band cannot be presented as a simple sum of isolated line profiles. Instead of that, a model accounting for

* Corresponding author. Fax: +7 8312 36 37 92.
E-mail address: trt@appl.sci-nnov.ru (M.Yu. Tretyakov).
URL: www.appl.sci-nnov.ru/mwl.

0022-2852/$ - see front matter © 2004 Elsevier Inc. All rights reserved.
doi:10.1016/j.jms.2004.11.011

the line mixing effect in the first-order approximation was suggested in [1]. According to that model the band absorption profile can be described by the following expression:

$$\alpha_{\text{band}}(f) = \sum_i C_i \cdot f^2 \cdot \left(\frac{\Delta v_i + Y_i \cdot (f - v_i)}{\Delta v_i^2 + (f - v_i)^2} + \frac{\Delta v_i - Y_i \cdot (f + v_i)}{\Delta v_i^2 + (f + v_i)^2} \right), \quad (1)$$

where the sum is over all lines in the band, i is the individual line index, f is current frequency, C_i is the line amplitude, Δv_i is the line half width at half maximum, v_i is the line central frequency, and Y_i is the line mixing parameter. The nonresonant component of absorption is included in the summation as $i = 0$, with $v_0 = 0$ and $Y_0 = 0$. The expansion in pressure was later carried to second order in [2].

To account for pressure and temperature dependence of the line broadening and mixing effects it is convenient to introduce normalized broadening γ_i and mixing coefficients y_i, relative to a temperature T_0 and independent of pressure, such that:

$$\Delta v_i = \gamma_i \cdot P \cdot \left(\frac{T_0}{T} \right)^x, \quad Y_i = y_i \cdot P \cdot \left(\frac{T_0}{T} \right)^x, \quad (2)$$

where P is the pressure, T is the temperature, and x is the temperature exponent for Δv_i. By this definition, y_i is potentially still a function of temperature, since Y_i may vary with temperature in a different way than Δv_i.

Precise knowledge of the 60-GHz oxygen absorption band parameters is demanded due to the importance of the band for atmospheric research, wireless communication, remote sensing, etc. Theoretical and experimental studies of the band have a long history, beginning in the first half of the last century [3–6]. These and later extensive studies resulted in development of an accurate millimeter-wave propagation model (MPM) [7] and its further improvement in 1992 [8]. An extended list of the oxygen band studies is given in [8].

Development of modern experimental techniques and methods [9–11] allows measurement of spectroscopic parameters of oxygen lines as well as absolute absorption value measurements with higher accuracy, which makes possible further improvement of atmospheric models. Some of the fine-structure transitions were studied in [12]. The present paper continues the series of our oxygen spectrum studies [9,11–14]. It includes precision measurement of central frequencies and pressure-broadening parameters of the 60-GHz band fine-structure transitions up to $N = 27$, and accurate wide-range measurement of the band absorption profile in pure oxygen and in laboratory air. The objective of this work is to obtain spectroscopic data of the 60-GHz band at a modern level of accuracy for atmospheric applications.

2. Low pressure experiment

A new experimental setup has been assembled for the study. The spectrometer and the measurement method are similar to those described in [9]. A block diagram of the experiment is presented in Fig. 1. The backward-wave oscillator (BWO) is of kind OB-70, stabilized by a phase lock-in loop against the 5th harmonic of an 8–18 GHz microwave synthesizer (RCh6-03, "Kvarz," Nizhny Novgorod). The minimal frequency step of the synthesizer is 20 kHz, corresponding to 100 kHz step of the BWO radiation. That is a bit more than desired for detailed observation of narrow oxygen line profiles at pressures below 1 Torr. So for scanning the BWO frequency we used one more frequency synthesizer in the range 1–110 MHz (Ch6-66, "Kvarz", Nizhny Novgorod), changing the intermediate frequency in the phase lock-in loop and thus providing any desirable BWO frequency steps from 200 Hz to a few MHz. Corresponding modification of the spectrometer controlling software was made. A PIN diode chops the BWO radiation at a modulation frequency of 180 Hz. The output signal of the radio-acoustic gas cell is demodulated by a digital lock-in amplifier, giving the signal of radiation absorption inside the cell. The cell was carefully demagnetized and screened by a double permalloy shield to avoid Zeeman splitting of oxygen lines by Earth's and other external magnetic fields. The cell was permanently connected to a vacuum system during experiments. Pressure in the system was controlled by a Type 627B 10-Torr range MKS Baratron having a declared accuracy of 0.12%. Pure (99.998 vol.%) oxygen and nitrogen samples were supplied by Messer MG Company. The experiment was carried out at room temperature measured by a Hg-based laboratory thermometer with 0.2 °C accuracy. From day to day and from morning to evening the slow temperature variations remained within 22–24 °C.

Each oxygen line was recorded scanning by frequency steps of the 1–110 MHz synthesizer. The value of the frequency step was chosen so the total scan length corresponded to about four full widths (FWHM) of the recorded line. Each line record contains 151 frequency/amplitude points. The time constant of the digital lock-in amplifier was near 0.06 s. Depending on the line strength, we made up to 40 amplitude measurements at every frequency and up to 12 back-and-forth frequency scans with further averaging of results to increase the signal-to-noise ratio. Examples of experimental records of the 7+ and 27+ lines in pure oxygen are shown in Fig. 2. The number of measurements averaged for the 27+ line was 240 times greater than for the 7+ line. The special feature of the present experiment was careful accounting of the baseline for each line record. The baseline signal arises in the RAD cell as a result of chopped radiation absorption in the cell windows,

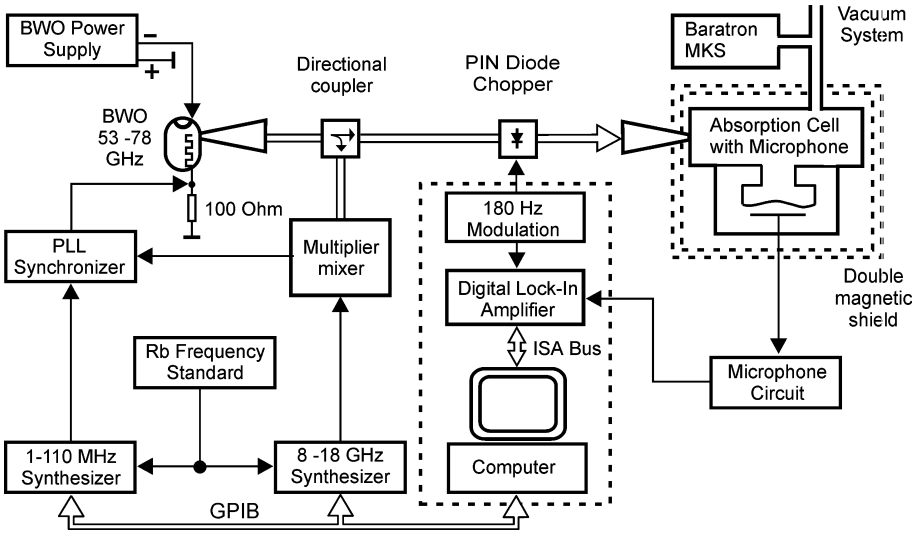

Fig. 1. RAD spectrometer block-diagram.

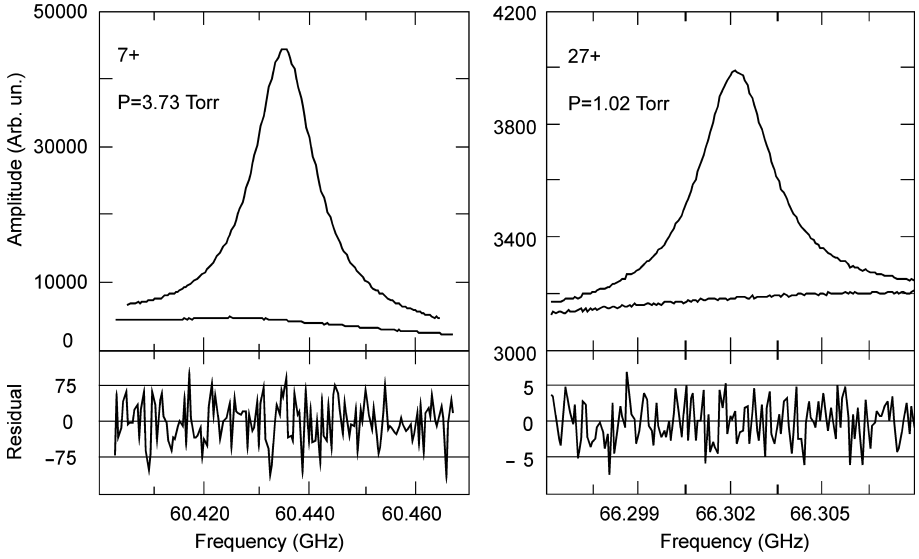

Fig. 2. Example of line with baseline and baseline only records (upper plots) and residuals of lines fitted to the model function (3) (lower plots). Both lines were recorded in pure oxygen at pressure shown in the figures.

microphone elements, etc., providing secondary gas heating and thus producing the synchronous-with-modulation microphone signal. This baseline signal adds to the signal of molecular absorption. Its value depends on radiation power and gas pressure in the cell. As shown in [11] this signal can be accounted for by filling the cell with non-absorbing gas (we used pure nitrogen having negligible absorption in this range) at the same pressure as the studied sample, repeating the record and subtracting the produced signal. Baseline records corresponding to 7+ and 27+ lines are also shown in Fig. 2. As seen from the figure, the baseline signal can constitute a small part of the molecular absorption signal or even considerably exceed it as in the case of the weak 27+ line, but the method allows practical elimination of the baseline influence on the shape of the observed line. For practical baseline accounting we experimentally determined the function describing dependence of the baseline signal on the gas pressure. This function is related to the gas cell properties and is independent of radiation frequency. For every oxygen line the baseline was recorded at the highest pressure of the experiment. Then the aforementioned function allowed calculating the baseline for sample records at any experimental pressure. Coincidence of two baselines recorded before and after the sample pressure variation experiment indicated a successful measurement.

After subtraction of the baseline from the line record, the following model function was fitted to experimental points:

$$I(v) = A_0 \cdot (1 + A_1 \cdot (v - v_0)) \cdot \Gamma(v - v_0) + A_2 + A_3 \cdot (v - v_0) + A_4 \cdot (v - v_0)^2. \quad (3)$$

The model represents a normalized line profile function $\Gamma(v-v_0)$ describing molecular absorption, a multiplicative term accounting for power dependence of the radio-acoustical signal and additive terms accounting for imperfection of the baseline subtraction. The A_i are adjustable coefficients. A Lorentz line-profile function was found to be sufficient. The line center frequency and the linewidth were determined from the fit. Residuals of the model (3) fitting to lines 7+ and 27+ are shown in the lower part of Fig. 2.

For each oxygen line the pressure broadening parameter was obtained from the result of linear regression of the linewidths recorded at 10–12 pressures in the range 0.2–4 Torr. At each pressure the line record was repeated 3–6 times to get higher accuracy and to estimate the statistical error of the measurement. For the oxygen broadening measurement we started from the highest sample pressure and then gradually pumped out the gas cell. For the nitrogen broadening parameter measurement we kept the partial pressure of oxygen in the cell near 1 Torr, adding nitrogen gradually up to a total pressure of 2–4 Torr. As an example, the dependence of linewidth (HWHM) versus total pressure inside the cell for the 11+ line is shown in Fig. 3, along with residuals of the linear regression. The intercept point of the regression line with the zero pressure axis is only +1.6 kHz for the self-broadened line, which means that remaining Zeeman and other parasitic line broadening effects are weak. As an estimate of broadening-parameter experimental error we took the limits of possible parameter deviation allowed by the experimental data; that usually corresponded to 4–6 standard deviations of the parameter obtained from the regression. Repeated measurements performed for a number of selected lines resulted in broadening-parameter variations within our estimated limits. It is worth mentioning that our results coincide, within experimental errors, with broadening parameters of a few selected lines measured in our previous work [12] by use of another RAD spectrometer.

Fig. 4 shows measured positions of the 11+ line center for the same experiment. The dependence indicates that linear-with-pressure shift of the line center does not exceed ±5 kHz/Torr as a most rigorous bound. No noticeable lineshift was observed for other oxygen lines, as well.

Oxygen line parameters obtained from these experiments, together with estimated errors in units of the last given digit, are presented in Table 1. The temperature exponent of $x = 0.8$ [8] was used for the temperature variation of linewidth and to recalculate all the data to the uniform temperature of 23 °C.

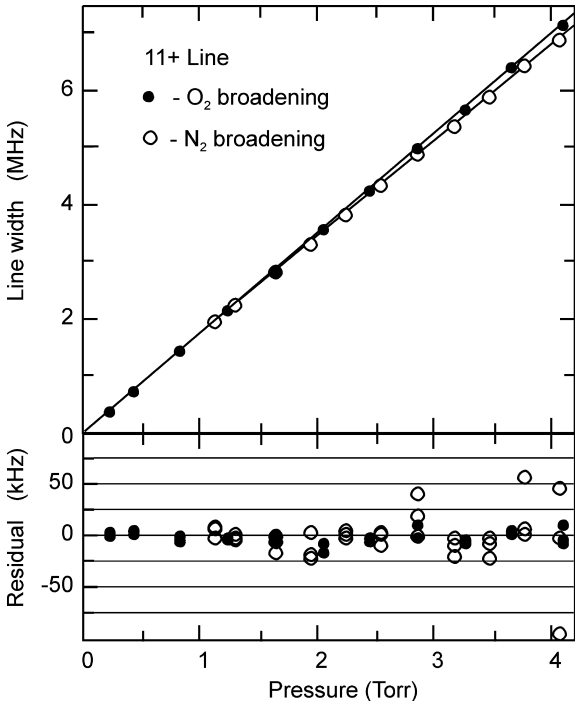

Fig. 3. Pressure broadening of 11+ line at 23 °C. Experimental points are shown by filled circles for O_2 and by open circles for N_2. Solid lines are the result of linear regression of the experimental points. Slopes of lines are 1.743(10) and 1.689(10) MHz/Torr. Residuals of the fit are shown below. Intercept for the self-broadened line is 1.6 kHz.

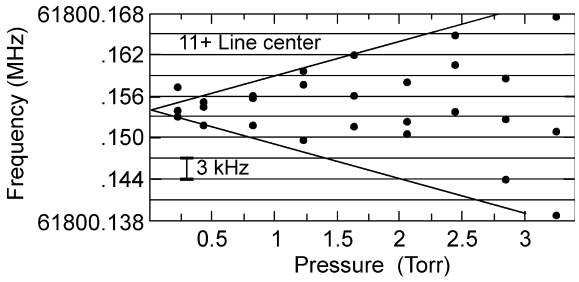

Fig. 4. Position of the line center frequency versus oxygen pressure for 11+ line. Measured frequencies are denoted by circles. Solid lines correspond to ±5 kHz/Torr linear-with-pressure shift.

3. Discussion of low-pressure experiment results

Broadening parameters measured in the present work are also displayed in graphical form in the upper part of Fig. 5. The figure reveals smooth decreasing of the broadening parameter with increasing of rotational quantum number. The $N-$ branch goes a little higher for low N but practically coincides with the $N+$ branch at higher N. Some evidence of rotational resonance slightly changing the rate of decrease of broadening is observed in the vicinity of $N \pm = 11$. It is interesting to note that N_2 broadening is larger than self-broadening for low N, but decreases more sharply with N and it crosses the self-broadening curve. As a consequence

Table 1
Measured parameters of the 60-GHz band lines at $T = 23$ °C

$N^{\pm}$	Measured frequency (MHz)	Obs. − Calc. (kHz)	Broadening parameter (MHz/Torr)	
			O_2	N_2
1^{-}[a]	118750.340(7)	6.4	2.230(10)	2.245(20)
1^{+}	56264.774(12)	3.0	2.238(17)	2.310(30)
3^{-}	62486.256(6)	2.9	2.067(10)	2.032(25)
3^{+}	58446.585(5)	−3.1	2.011(10)	2.008(15)
5^{-}	60306.053(5)	−3.3	1.920(10)	1.904(15)
5^{+}	59590.983(5)	3.0	1.890(10)	1.900(12)
7^{-}	59164.204(4)	0.0	1.834(8)	1.820(10)
7^{+}	60434.777(4)	−0.8	1.816(12)	1.802(10)
9^{-}	58323.876(4)	−0.7	1.763(15)	1.740(13)
9^{+}	61150.563(4)	0.8	1.767(10)	1.734(30)
11^{-}	57612.487(4)	0.8	1.743(10)	1.689(10)
11^{+}	61800.153(6)	−5.1	1.747(10)	1.690(10)
13^{-}	56968.212(4)	0.6	1.693(10)	1.637(17)
13^{+}	62411.221(4)	0.6	1.701(10)	1.624(15)
15^{-}	56363.397(5)	−1.7	1.673(10)	1.584(10)
15^{+}	62997.984(4)	0.4	1.668(15)	1.559(10)
17^{-}	55783.813(6)	−2.1	1.624(10)	1.502(18)
17^{+}	63568.524(4)	−1.6	1.619(10)	1.504(10)
19^{-}	55221.386(5)	1.7	1.586(15)	1.452(40)
19^{+}	64127.777(4)	2.3	1.577(15)	1.421(15)
21^{-}	54671.184(7)	4.1	1.541(20)	—
21^{+}	64678.912(10)	1.6	1.542(12)	—
23^{-}	54130.031(15)	6.5	1.520(40)	—
23^{+}	65224.077(5)	−0.9	1.484(20)	—
25^{-}	53595.777(17)	1.6	1.464(25)[b]	—
25^{+}	65764.774(12)	−4.7	1.460(20)[b]	—
27^{+}	66302.098(12)	1.7	1.399(30)[b]	—

[a] Measured in previous work [11].
[b] Estimated value from the line records at 1 Torr.

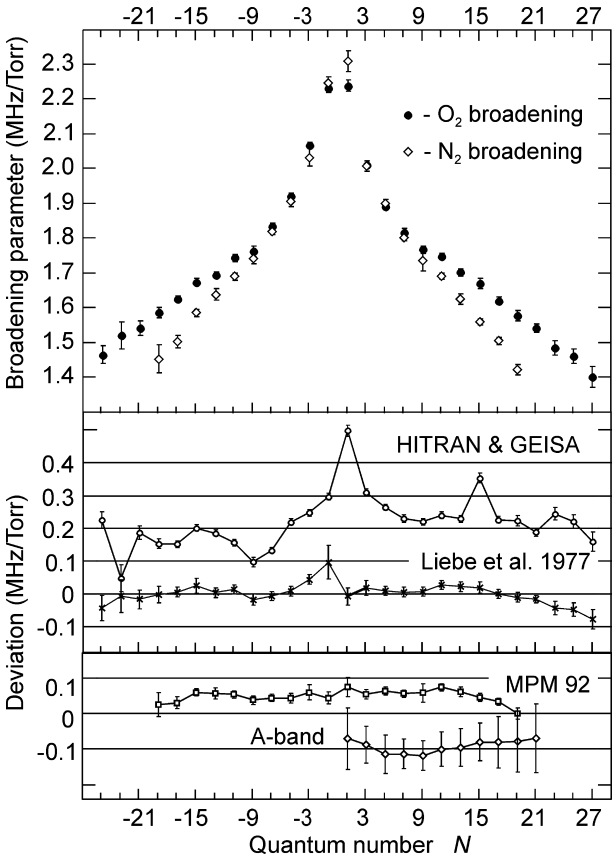

Fig. 5. Pressure broadening parameters measured in the present work (upper plot) and their comparison with some other known data (lower plot). Our experimental points in upper plot are denoted by bullets for O_2 (self-) broadening and diamonds for N_2 broadening. Estimated experimental errors are shown by vertical bars. Two lower plots present differences between our data and corresponding values found from various sources: HITRAN/GEISA (circles), work of Liebe et al. [19] (crosses) and MPM92 (boxes). The lowest trace (diamonds) is a comparison with broadening of corresponding lines of the oxygen A-band at 760 nm (see explanations in the text).

of such behavior the efficiency of air broadening (air- to self-broadening ratio) of oxygen lines differs from line to line, varying from 0.92 to 1.03. Early works of Liebe (see e.g. [15] and references therein) are in good agreement with our results on this point. These experimental results contradict data in the most recent versions of the databases HITRAN (version 2004) [16] and GEISA (version 2003) [17]. Both databases give exactly the same self- and air-broadening parameters for the oxygen lines, and a constant efficiency of 1.02. The difference between our measured self-broadening coefficients and corresponding values from the databases is presented by circles (upper trace) in the middle part of Fig. 5. The large systematic divergences and the random deviation from line to line demonstrate a need to update these linewidths in HITRAN and GEISA.

The difference between air-broadening calculated from our measurements as $0.21 \cdot \gamma_{O_2} + 0.79 \cdot \gamma_{N_2}$, and corresponding data from MPM92 [8] is presented by boxes in the lower part of Fig. 5, showing very good agreement. The small positive offset of about 50 kHz/Torr on average would be eliminated if all MPM broadening data were multiplied by a factor of 1.033. The multiplication slightly reduces the standard deviation of the difference as well. This is also in agreement with the authors of MPM92 mentioning in their work [8] that multiplication of the widths by a factor of 1.05 and corresponding correction of mixing coefficients slightly improved agreement of the model with their experiments. (This adjustment was later included in the MPM93 model [18].)

Even better agreement (within estimated errors of both experiments) is found between our self-broadening data and experimental results of [19] (shown by crosses), which validates both studies since the data are obtained by essentially different techniques.

We also compared our self-broadening data with self-broadening of the oxygen A-band lines at 760 nm. The description of the comparison method follows. Fine-structure transitions forming the 60-GHz band are within the $X^3\Sigma_g^+$ ground electronic state, while the A-band lines arise from the $b^1\Sigma_g^+ \leftarrow X^3\Sigma_g^+$ electronic transition of molecular oxygen. All transitions allowed by selection

Table 2
Transitions N', $J' \leftarrow N$, J allowed for any lower level N for A- and 60 GHz-bands

A-band	60 GHz-band
$N-1, N-1 \leftarrow N, N$	
$N-1, N-1 \leftarrow N, N-1$[a]	$N, N \leftarrow N, N-1$
$N+1, N+1 \leftarrow N, N$	$N, N \leftarrow N, N+1$
$N+1, N+1, \leftarrow N, N+1$	

[a] Except $N = 1$.

rules for any lower level N for the fine-structure band and for the A-band are presented in Table 2.

This unusual presentation of transitions allows one to see that line-broadening of these two bands can be compared using the lower-level N as a common parameter. All levels involved in both series of the 60-GHz transitions are also involved in the four series of corresponding A-band transitions. Keeping in mind that the line broadening equally depends on both lower and upper level lifetimes and the monotone dependence of the broadening on quantum number, it seems logically justifiable to compare averaged broadening of two 60 GHz lines with averaged broadening of four A-band lines having the same lower level N. Differences between our data and A-band self-broadening data from [20], averaged as explained above are presented by diamonds (lower trace) in the lower part of Fig. 5. The small negative 100 kHz/Torr offset of the differences is perhaps related to an unknown influence of the $b^1\Sigma_g^+$-state-levels' lifetimes. The small difference, being practically constant within measurement errors, demonstrates very good agreement of both data sets, which confirms the similarity of broadening dependence on quantum number N for different kinds of oxygen transitions.

Table 3
Molecular constants for $^{16}O_2$ in $^3\Sigma_g$ ground electronic and vibrational state

Constants	This work (MHz)	Ref. [14] (MHz)
B_0	43100.4425(12)	43100.4425(12)
D_0	0.145123(13)	0.145124(13)
H_0	$3.8(36) \times 10^{-8}$	$3.8(36) \times 10^{-8}$
λ	59501.3435(16)	59501.3456(26)
λ_D	0.058369(10)	0.058344(17)
λ_{DD}	$2.899(92) \times 10^{-7}$	$3.13(14) \times 10^{-7}$
γ	−252.58633(18)	−252.58648(34)
γ_D	$-2.4344(68) \times 10^{-4}$	$-2.452(11) \times 10^{-4}$
γ_{DD}	$-1.45(47) \times 10^{-9}$	$-1.57(71) \times 10^{-9}$

Numbers in parentheses correspond to the standard deviation in units of the last digit quoted.

We did not aim at precise measurement of oxygen line center frequencies, which are well known from previous work (see e.g. [14] and references therein). Nevertheless it turned out that our frequencies, obtained as a useful byproduct of the experiment, have somewhat higher accuracy compared to previously known data. Moreover, to the best of our knowledge the 21+ and 27+ lines were not measured previously. The new frequencies were fitted, together with all previously measured oxygen lines from microwave to far infrared, using the program "SPFIT.EXE" from JPL [21] by analogy with fitting reported in [14]. Differences between observed and calculated frequencies are shown in Table 1. A new set of molecular constants was obtained; see Table 3 for the comparison with previously known [14] constants.

As expected, the accuracy and value of the pure rotational constants remained the same, but we gained about 60% of accuracy in the fine-structure constants. A clear improvement in accuracy of central line frequencies is demonstrated in Fig. 6, where author-estimated experimental frequency accuracy, absolute value of deviation between observed and calculated frequencies, and frequency prediction errors are shown for all fine-structure lines including high-N lines measured by other

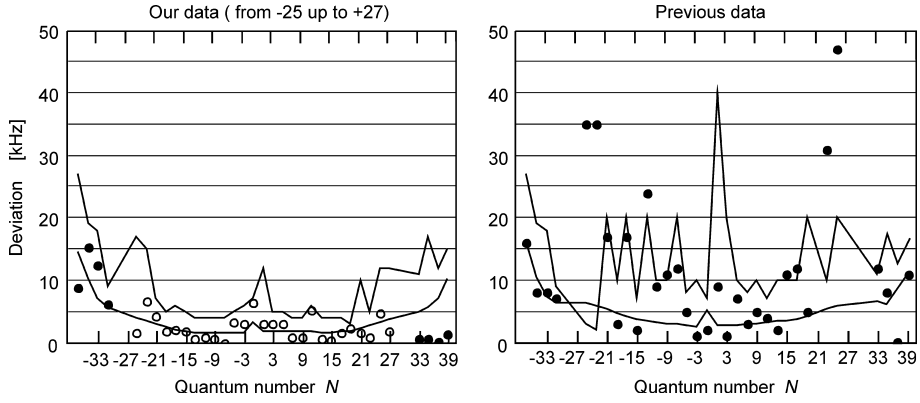

Fig. 6. Result of fitting of the 60-GHz band measured line central frequencies to theoretical model. Left plot, our data including previously known data for high N lines. Right plot, previously known ([14] and references therein) data. Circles, absolute value of difference between observed and calculated frequency. Open circles, our data; filled circles, previous data. Upper trace, experimental frequency errors estimated by authors. Lower trace, calculated frequency error.

authors. The same plot for previously known data is shown on the right side for comparison.

4. Atmospheric pressure experiment

The resonator spectrometer with fast digital frequency scanning described in [10] and method of absolute absorption measurement using sample substitution by non-absorbing gas described in detail in [11,22] were employed.

The sample absorption coefficient α measured by our resonator spectrometer at frequency points corresponding to eigen-frequencies of the resonator can be expressed (assuming $\alpha L \ll 1$, L is the resonator length, which corresponds to our case since even in pure O_2 in the band center $\alpha L \sim 4 \times 10^{-4}$) as

$$\alpha = (2\pi/c)(\Delta f - \Delta f_0), \tag{4}$$

where Δf and Δf_0 are, respectively, widths of the Fabry–Perot resonance with sample and filled by non absorbing gas (pure nitrogen), directly measured in the experiment, and c is the speed of light.

Radiation absorption at room temperature varying within 21–23 °C was measured at 82 frequencies in the range 45–96 GHz for laboratory air, pure oxygen, and pure nitrogen (the last called the spectrometer baseline record) at atmospheric pressure varying within 751–759 mmHg. To exclude accidental influence of any unknown factor, the records were repeated three times each.

The resonator spectrometer experiment consumed large amounts of sample gases to fill the resonator and to maintain permanent sample conditions during the experiment. So instead of pure gases, inexpensive commercially available cylinders with technical grade nitrogen and oxygen from a local supplier were used. The technical director of the supply firm informed us that the usual purity of the oxygen gas is 99.7 vol.%, although contamination during filling of cylinders could occasionally reduce it as low as 98%. Remaining water content was 0.65–0.75 g/m^3 during the O_2 experiment, 8.7–9.5 g/m^3 during the air experiment, and 0.8–1.2 g/m^3 during the baseline recording. Temperature (T), pressure (P), and humidity (H) variation during the experiment were taken into account and the absorption for average T_0 and P_0 during the experiments and zero humidity was recalculated from the experimental data using MPM92 as described below.

The sample absorption coefficient α can be divided into three parts

$$\alpha = \alpha_{O_2} + \alpha_{water} = \alpha_0 + \Delta\alpha_{O_2} + \alpha_{water}, \tag{5}$$

where α_0 corresponds to the absorption coefficient of oxygen in the sample at permanent conditions of the sample, ($T_0 = 295.15$ K, $P_0 = 755$ mmHg, $H_0 = 0$ g/m^3 for air and $T_0 = 295.95$ K, $P_0 = 758$ mmHg, $H_0 = 0$ g/m^3 for pure oxygen) and $\Delta\alpha_{O_2}$ is the variable part of the absorption due to variations of aforementioned parameters in the course of the experiment. This part was calculated using MPM92 [8] as:

$$\Delta\alpha_{O_2}(T,P,H,f) = \alpha_{O_2}(T,P,H,f) - \alpha_{O_2}(T_0,P_0,H_0,f). \tag{6}$$

A scaling coefficient accounting for increased absorption was used for the pure oxygen sample. The water absorption part was calculated as in [23]

$$\alpha_{water} = \alpha_{H_2O}(T,P,H,f). \tag{7}$$

Then the sample absorption coefficient at permanent conditions was expressed as

$$\alpha_0 = \alpha - \Delta\alpha_{O_2} - \alpha_{water}. \tag{8}$$

With this adjustment the repeated experimental records of the sample absorption practically coincided within experimental noise. Resulting absorption profiles in air and pure O_2 were obtained by averaging of repeated records.

Results of the experiment are presented in the upper part of Fig. 7. The middle part of the figure presents a comparison of the measured dry air absorption profile with MPM92 calculations. The difference trace (diamonds) reveals very good general agreement between observed and calculated spectra, with small deviations

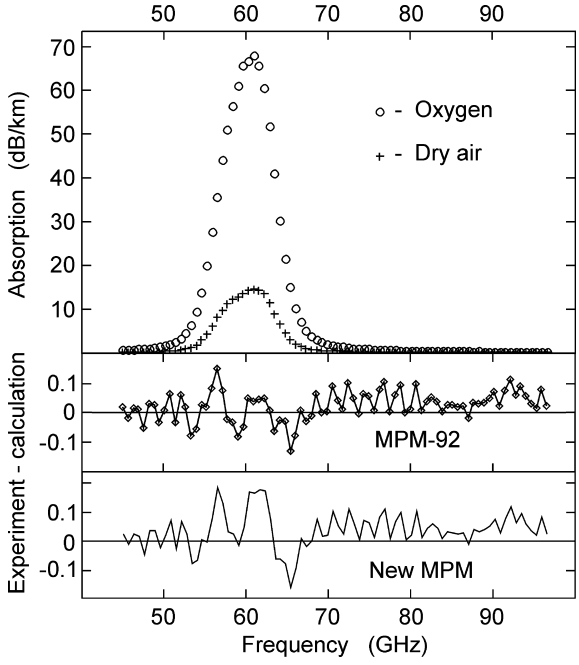

Fig. 7. Experimentally measured 60 GHz O_2-band absorption profile in pure oxygen (o) and air (+) at room temperature and atmospheric pressure and its comparison with calculation using: (a) MPM92 as it is (diamonds) and new MPM with parameters obtained in course of this work (solid line with no points marked).

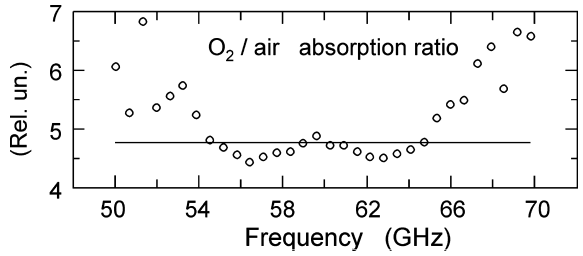

Fig. 8. Ratio of measured absorption in pure oxygen over absorption in air (circles). The solid line corresponds to the ratio of oxygen content in the gas sample during experiments (0.997/0.20946).

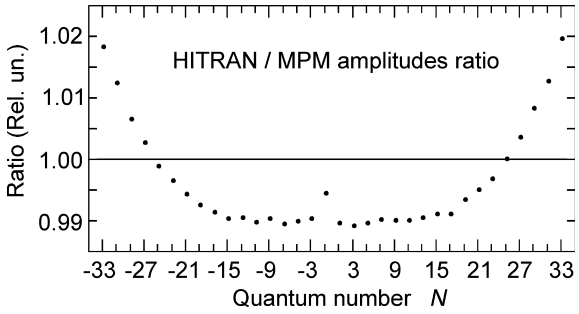

Fig. 9. The ratio of oxygen line intensities from HITRAN to ones used by MPM versus quantum number.

on the band slopes exceeding the noise level by about a factor of 2, confirming both the quality of the experiment and the accuracy of the model. The small positive bias of the difference at first glance looks like under-accounting of water vapor absorption. In principle it could be eliminated by increasing the water content during air measurements by about 1 g/m^3, but this is about twice the possible absolute humidity measurement error derived from uncertainties declared by the manufacturer of our meter "TESTO-645" [24]. Detailed analysis of the data during derivation of mixing coefficients described below also confirms that extra water absorption is an unlikely reason and the bias is probably related to some unknown systematical error of our experiment. The lower panel of Fig. 7 presents comparison of the experimental result with calculation using updated in course of the present work model. The residuals also contain some systematic deviations near the band center due to second-order mixing, which is discussed in the next section.

The ratio of absorption coefficient in air to absorption in pure oxygen in the most informative range 50–70 GHz is shown in Fig. 8. The solid line in the figure corresponds to the ratio of oxygen content in the gas sample during experiments (0.997/0.20946). The clear systematic variation of the absorption ratio in the vicinity of the band center is related to the difference of collisional line parameters between pure oxygen and air. Farther from the band center the air absorption becomes small and comparable with experimental noise so the ratio is not as reliable.

5. Mixing coefficients

Our low-pressure measurements indicate a need to update the oxygen line widths in MPM. It was also decided to update the O_2 line intensities to those of the more modern calculation of [25], which have been incorporated into the HITRAN database. These are ~1% weaker for low values of N, and ~2% stronger for higher N, compared to the MPM92 line intensities. The ratio of new intensities to ones from MPM92 is shown in Fig. 9. The newer widths and intensities promise improved accuracy of model calculations at low pressures where the lines are resolved, but they are not consistent with the MPM92 mixing coefficients. To maintain the model accuracy at higher pressures, we used our atmospheric-pressure data to derive new mixing coefficients that are compatible with the updated widths and intensities.

As described in [8], the MPM92 mixing coefficients were derived by a method that adjusted the coefficients to minimize the quantity

$$\sum_{j=1}^{n} \varepsilon_j^2 + \beta q, \tag{9}$$

where the ε_j, $j = 1,\ldots,n$ are residual differences between measured and calculated absorption for n measurements, q is a quadratic measure (defined in [8]) of structure in the rotational relaxation matrix, and β is a Lagrange multiplier, whose value is chosen from the tradeoff curve (e.g., see Fig. 3 in [8]) between minimization of structure and minimization of residuals.

We expect small differences from MPM92, so in the present work we substituted the normalized mixing coefficients y_i of MPM92 for the bias values defined in [8, Eq. (20)]. The bias term was originally introduced in [26] as a way of accounting for mixing between the positive-frequency, zero-frequency (or nonresonant), and negative-frequency branches of the fine-structure spectrum, while the fitting algorithm adjusted the intra-branch mixing. Since the MPM92 mixing coefficients include the contribution from this bias, they are acceptable as a baseline for a new derivation of the y's. Fig. 10 shows the standard deviation of the difference of measured absorption in pure O_2 minus absorption calculated with new mixing coefficients y_i derived from the experiment, as the value of β is varied. Very large values of β drive the derived y-coefficients to the MPM92 values, with corresponding maximum residual variance. As β is lowered, the mixing coefficients are modified to reduce the residuals. Typically the residuals begin to level off, at the point we call the "knee." The fact that the residuals continue to decrease with decreas-

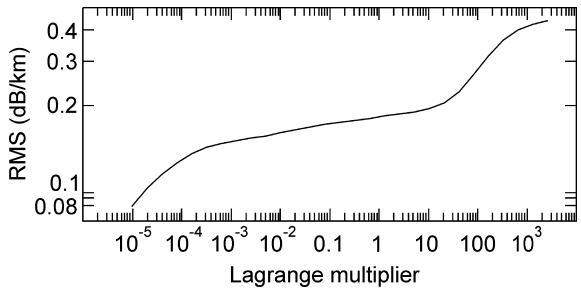

Fig. 10. Standard deviation of observed minus calculated absorption profile versus normalized Lagrange multiplier (β/n) for the pure oxygen experiment ($n = 82$) in logarithmic scale. The "knee" is in vicinity of $\beta/n = 20$.

ing β, although at a slower rate, instead of leveling off at a true noise floor, is a symptom of some systematic discrepancies that are not easily fitted by the model. Further lowering of β leads to a second change of slope where the systematic errors are being wiped out and the residual represents pure experimental noise. There is also a reverse change of slope at high β where the residuals approach the value with no fitting, and the resulting mixing coefficients approach the MPM92 values.

For deriving the mixing coefficients and for comparison with the experiment, the calculated absorption was multiplied by 1.0053. The origin of the factor is as follows. MPM calculates absorption from the ground state lines of the $^{16}(O_2)$ isotope. The natural isotopic abundance of the species is 0.9952. The fraction of $^{16}(O_2)$ molecules in the first exited state at room temperature can be calculated using Boltzmann factor as 0.0005. Thus the fraction of molecules accounted for by the model is 0.9947. We did not have a model for mixing of lines from the other isotopomers of O_2, but on the assumption that they would have a similar band shape to that of $^{16}(O_2)$ when overlapped at atmospheric pressure (modeling the absorption profiles using HITRAN data confirms the similarity), we multiplied the calculated absorption by $(0.9947)^{-1}$ to approximately account for contributions from the other isotopomers and excited-state lines.

In preliminary trials of the fitting method with the pure-O_2 data, we varied the oxygen content assumed for the calculation of absorption and found the smallest residual errors with a volume fraction of 0.999 O_2. That value is close to the supplier's 0.997, so we used the latter value in the subsequent analyses. The left panel of Fig. 11 shows the observed minus calculated residuals at $\beta/n = 20$ (10^5 Pa dB/km), where we found the "knee" of the residual variance. It is evident from this figure that the residuals contain some systematic discrepancies with the model, in addition to measurement noise. Fig. 12 illustrates one potential source of such model

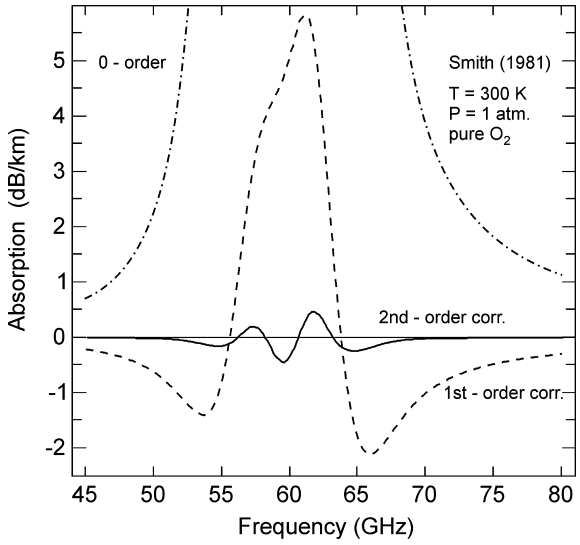

Fig. 12. First- and second-order line mixing contributions to absorption in pure O_2 at 1 atm. pressure, calculated from the model of [2]. The first-order correction (dashed line) is the absorption calculated using first-order mixing only, minus absorption calculated without mixing. The second-order curve (solid line) is the absorption with first- and second-order mixing, minus absorption with first-order mixing. The zero-order contribution (dash-dot line) peaks at 56 dB/km near 61 GHz.

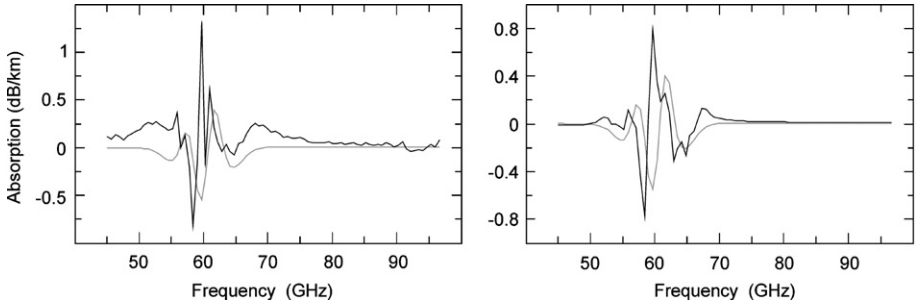

Fig. 11. Left panel: the black trace is measurement minus model residuals for pure oxygen. The smooth gray curve is the component of theoretical second-order line mixing that is orthogonal to the first-order mixing. Right panel: the black trace is difference of residuals corresponding to the "knee" point ($\beta/n = 20$) and to the point where the residual presents experimental noise ($\beta/n = 10^{-4}$). The smooth gray curve is the same function as in the left panel.

discrepancy, which is the contribution of line mixing higher than first order in pressure. The curves in Fig. 12 are calculated from the second-order line mixing theoretical model of Smith [2]. (We corrected an error in Eqs. (17) and (18) of [2], where the second-order lineshift $\delta\nu_k$ should enter with the same sign as ν_k.)

The second-order contribution is not perfectly orthogonal to the first-order curve; therefore, we consider that some part of second-order line mixing has contributed to the derived first-order coefficients and does not show up in the residuals. To estimate this effect, we calculated the first-order mixing contribution in our experimental record (i.e., model calculated absorption minus Van Vleck–Weisskopf component). Then we used the Gram–Schmidt procedure to obtain components of the second-order mixing contribution (calculated with Smith's coefficients) parallel and orthogonal to the first-order curve. The parallel component (projection of the theoretical second-order curve onto the fitted first-order mixing) amounted to ~0.9% of the first-order mixing contribution. The orthogonal component (the difference between the theoretical second-order curve and the parallel component) is shown by the smooth curve in Fig. 11. The right panel of Fig. 11 compares the orthogonal component to the difference of residuals corresponding to $\beta/n = 20$ and $\beta/n = 10^{-4}$ (where the residual presents experimental noise as explained earlier). This difference removes most of the experimental noise and reveals systematic variations relative to the model. In both panels there is a general similarity of the calculated curve (shown as a smooth gray curve) to the residuals, though not a precise correspondence, and the residuals at 58.3 and 59.5 GHz appear to be larger in magnitude due to some other cause.

Similar calculations were performed for the air experiment. Although in this case we just scaled the theoretically calculated (for pure O_2) second-order mixing contribution to get a qualitative picture. The results are shown in Fig. 13. Again both panels reveal a general similarity of the second-order contribution and residuals.

The results shown in Figs. 11 and 13 indicate a need to consider error due to higher-order mixing effects not included in the model. It appears that the absolute value of the model error is maximal in the vicinity of the absorption band center and decreases on the band wings. So we adopted the following estimate of rms uncertainty for model errors at 1 atm. pressure

$$E_{\text{model}}(f) = 0.5 \cdot a_{O_2} \cdot \exp[-0.03 \cdot (f - 60.5)^2](\text{dB/km}), \tag{10}$$

where a_{O_2} is the fractional abundance of oxygen and f is the frequency in GHz.

The right panel of Fig. 14 compares the model error function (smooth gray curve) to the absolute value of the second-order mixing effect from Fig. 12 (black curve).

Up to this point, the experimental errors were treated as having stationary statistics. However the data analysis indicated that the pure oxygen experiment had increased experimental noise near the absorption band center. This was because of decreased signal-to-noise ratio due to increasing radiation absorption inside the resonator filled by pure oxygen. On the other hand, the air experiment had quite uniform noise over the entire frequency range. The following model function was adopted for rms experimental noise:

$$E_{\text{exp}}(f) = \sigma + 0.5 \cdot 10^{-0.21 \cdot |f - 59.4|^3} \quad \text{(pure oxygen)} \tag{11a}$$

$$E_{\text{exp}}(f) = \sigma \quad \text{(air)} \tag{11b}$$

where σ is the estimated rms measurement noise outside the absorption band, considered to be 0.05 dB/km for pure oxygen and 0.04 dB/km for air. The left panel of Fig. 14 compares the experimental noise function (smooth gray curve) to the absolute value of differences between three repeated pure O_2 absorption records (black curves). After introducing those error functions (10) and (11a)(11b), the line-mixing fitting algorithm of [8] was modified by dividing both the absorption α and weighting matrix $\mathbf{W}$ by a factor s_j, as in

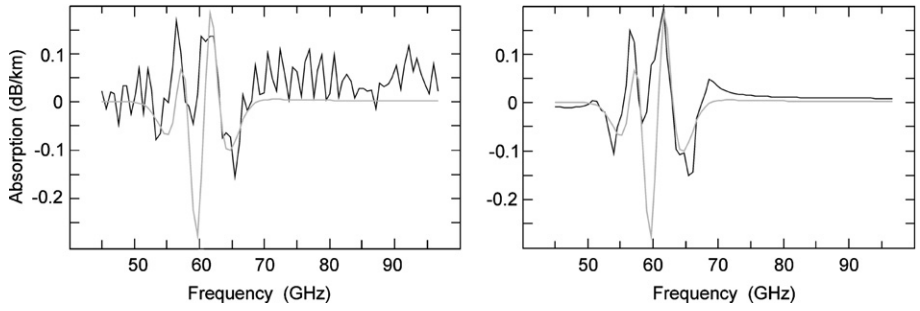

Fig. 13. Analog of Fig. 11 for the air experiment. Left panel: The black trace is measurement minus model residuals for air. The smooth gray curve is the component of theoretical second-order line mixing that is orthogonal to the first-order mixing. Right panel: The black trace is difference of residuals corresponding to the "knee" point and to the point where the residual presents experimental noise. The smooth gray curve is the same function as in the left panel.

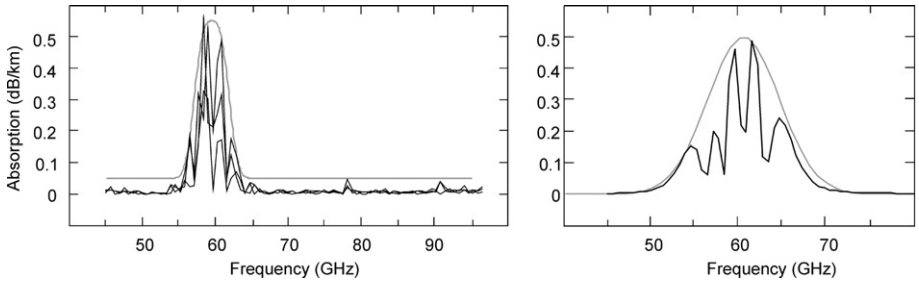

Fig. 14. Left panel: The oxygen experiment error function $E_{\text{exp}}(f)$ (smooth gray curve) and absolute value of differences between three repeated pure O_2 absorption records. Right panel: The model error function $E_{\text{model}}(f)$ (smooth Gauss curve) and absolute value of the calculated influence of the second-order mixing effect (lower curve) in frequency range of oxygen absorption band.

$$\left(\alpha_j - \alpha_j^b\right)/s_j = \sum_i \left(W_{ji}/s_j\right) \cdot (y_i - b_i) + \varepsilon_j, \tag{12}$$

which replaces [8, Eq. (19)]. In the above, α_j is measured absorption at frequency f_j, α_j^b is absorption calculated using the baseline mixing coefficients b_i (which in the present case are the MPM92 coefficients), and s_j is calculated as

$$s_j = \frac{1}{\sigma} \cdot \sqrt{E_{\text{exp}}^2(f) + E_{\text{model}}^2(f)}. \tag{13}$$

The effect of this modification is to pre-whiten, or equalize the variance of the residuals, which the fitting algorithm seeks to minimize; consequently it reduces the influence of measurements at those frequencies where the errors are expected to be larger. Thus our objective is not to fit the experimental data as well as possible at all frequencies with the first-order model, but rather to derive coefficients that accurately describe the first-order mixing effect, which we know is only one part, although the largest, of the total phenomenon at one atmosphere pressure.

We believe that the influence of higher-order mixing on the MPM92 derivation [8] was minimized by a combination of factors. Those mixing coefficients were derived from measurements at a pressure of 701 hPa, which would reduce the magnitude of higher-order mixing compared to first order. Experimental residuals at the 701 hPa pressure were 0.15 dB/km rms, which is larger than the expected contribution of second-order mixing in air at that pressure.

Also, the slightly smaller linewidths and different line intensities used in [8] would have had an effect on calculated absorption in the same sense as line mixing, and to some extent would have compensated for the neglect of higher-order mixing. The influence of these factors explains the very good correspondence of the MPM92 calculation to our experiment (middle panel of Fig. 7). The lower part of Fig. 7 shows the difference between measured air absorption and model calculations using the new line parameters. It can be seen that at one atmosphere pressure the MPM92 line parameters yield a slightly better fit to the absorption near the band center, due to the differences in widths and intensities as discussed above. On the band wings, the two models yield very similar results. The new model gives about 0.5% less absorption in the 20–30 GHz range.

Mixing coefficients obtained by solution of Eq. (12) for the two atmospheric-pressure experiments are listed in Table 4. With the modified algorithm, we used

Table 4
Normalized mixing coefficients for pure oxygen and air

Quantum ID	y, pure O_2 ($1/10^5$ Pa)	y, air ($1/10^5$ Pa)
1−	−0.0350[a]	−0.0360[a]
1+	0.2314	0.2531
3−	−0.3408	−0.3641
3+	0.5111	0.5474
5−	−0.5243	−0.5685
5+	0.5657	0.6168
7−	−0.3568	−0.4214
7+	0.2800	0.3471
9−	−0.0832	−0.1489
9+	−0.0211	0.0420
11−	0.1124	0.0740
11+	−0.2035	−0.1714
13−	0.2935	0.3012
13+	−0.3686	−0.3841
15−	0.3668	0.4277
15+	−0.4246	−0.4929
17−	0.3947	0.5064
17+	−0.4406	−0.5582
19−	0.3978	0.5561
19+	−0.4355	−0.5979
21−	0.4238	0.6256
21+	−0.4561	−0.6601
23−	0.4589	0.6982
23+	−0.4872	−0.7268
25−	0.4696	0.7396
25+	−0.4949	−0.7632
27−	0.4714	0.7657
27+	−0.4941	−0.7851
29−	0.4885	0.8021
29+	−0.5090	−0.8178
31−	0.5124	0.8416
31+	−0.5306	−0.8537
33−	0.5358	0.8787
33+	−0.5517	−0.8869

[a] Measured in previous work [11].

$\beta/n = 2$ (10^5 Pa dB/km) for air and 0.5 for pure O_2. For consistency with MPM92, the coefficients are normalized with $T_0 = 300$ K in Eq. (2). These coefficients are compared to those of [8] and [2] in Fig. 15. In pure oxygen, the y-values are significantly (50–100%) larger than the first-order coefficients calculated in [2]; yet, as discussed above, the residuals apparently due to higher-order mixing in our pure-O_2 experiment were not much larger than the theoretical second-order effect. This difference indicates that a simple scaling of off-diagonal elements of the rotational relaxation matrix would not suffice to reconcile the theory with the measurements. In air, the newly derived mixing coefficients are generally a few percent larger in magnitude than those of MPM92, compensating for the small differences in linewidths and intensities. The derived values in air and pure oxygen are close together at values of $N \leqslant 13$, but diverge at higher N, which presents an interesting similarity to the behavior of the line widths shown in Fig. 5. (However, if the O_2 concentration were 98%, which we do not believe to be the case, then the mixing coefficients for pure O_2 would have come out very close to the values for air at all N.)

It should be pointed out that solving Eq. (12) for the y's is an ill-conditioned problem when the lines overlap. Therefore, the solution is not unique, unlike the case in [11] where it was possible to find the mixing coefficient for a single line. Rather, the coefficients derived here constitute a set, which as a whole satisfy the measurements with minimal departures from the baseline values b_k. This consideration was a further motivation for the use of MPM92 mixing coefficients as the baseline for the new derivation; by this means, the necessary changes to the model were minimized.

As the observed frequency approaches infinity, Eq. (1) approaches an asymptotic value given by

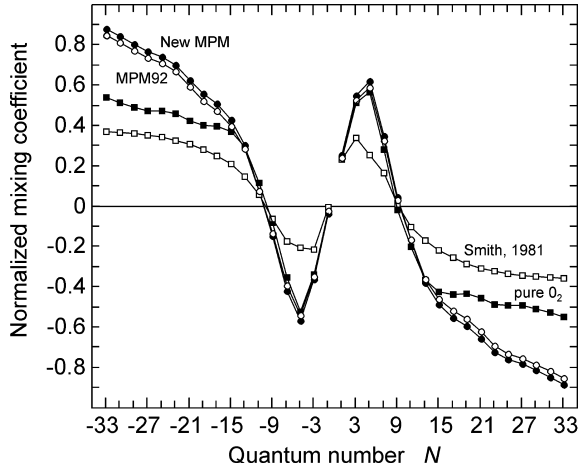

Fig. 15. First-order mixing coefficients for air (circles) and pure O_2 (squares). Filled circles and squares are the values obtained in this work. White circles are MPM92 mixing coefficients. White squares are mixing coefficients calculated by Smith [2].

$$\alpha_{\text{band}}(\infty) = 2 \cdot \sum_i C_i \cdot (\Delta\nu_i + Y_i \cdot \nu_i). \tag{14}$$

The fitting algorithm does not have any explicit constraint on this asymptote, and for the air experiment, it turns out to be -4×10^{-4} dB/km. Although extremely small, its negativity is of course nonphysical. In the pure oxygen experiment, the asymptote was $+1.4 \times 10^{-2}$ dB/km. For comparison, the MPM92 line parameters yield an asymptote of -4×10^{-4} dB/km, and MPM93 -4×10^{-3} dB/km, at 1 atm. and 295 K. These numbers do not include the contributions of the submillimeter lines to absorption. The different values may simply reflect experimental error. However, it is also true that the present model for line mixing does not consider the possibility of mixing involving the submillimeter oxygen lines, which could affect the asymptote value of the fine-structure band. It does include mixing between the resonant and nonresonant lines, which results in the sum given by Eq. (14) being less than the nonresonant contribution alone.

6. MPM update

MPM92 [8] defines line coefficients $a_1 \ldots a_6$ (adjusted to $T_0 = 300$ K) for calculation of complex refractivity. Line intensity is given as

$$S_{\text{MPM}_i} = a_1 \cdot 10^{-6} \cdot P \cdot (T_0/T)^3 \cdot \exp[a_2 \cdot (1 - T_0/T)], \tag{15}$$

which is related to the line amplitude in Eq. (1) by

$$C_i = 0.182 \cdot S_{\text{MPM}_i}/\nu_i \tag{16}$$

for absorption in dB/km and pressure in kPa. As previously stated, we derived a_1 and a_2 for the updated model from the HITRAN database. The MPM width coefficient a_3 is our γ_i (linearly extrapolated from experimental values for high N lines). For the present, we assume that all linewidths have the same temperature dependence ($x = 0.8$), hence $a_4 = 0$. As noted in the discussion of Eq. (2), the y_i may have some temperature dependence that is not removed by their normalization. In MPM92, this is modeled as

$$y_i = a_5 + a_6 T_0/T. \tag{17}$$

With measurements at only one temperature, we chose to retain a_6 from MPM92 and adjust a_5 to agree with the y's derived at 22 °C; this is equivalent to

$$y_i(T) = y_i(295.15) + a_6 \cdot [T_0/T - T_0/295.15], \tag{18}$$

thus a_6 appears as a temperature correction factor. Table 5 lists the updated coefficients for MPM. The line frequencies are calculated with the new set of molecular constants in Table 3. We did not attempt to add second-order line mixing to MPM. The second-order effect is maximized at pressures near 1 atm. and frequencies near

Table 5
Updated MPM coefficients for air

Quantum ID	ν_i (GHz)	a_1	a_2	a_3 (GHz/10^5Pa)	a_5 (1/10^5Pa)	a_6 (1/10^5Pa)
1−	118.750334	940.3	0.010	1.664[a]	−0.0439[a]	0.0079
1+	56.264774	543.4	0.014	1.703	0.3525	−0.0978
3−	62.486253	1503.0	0.083	1.513	−0.4499	0.0844
3+	58.446588	1442.1	0.083	1.491	0.6768	−0.1273
5−	60.306056	2103.4	0.207	1.415	−0.6395	0.0699
5+	59.590983	2090.7	0.207	1.408	0.6957	−0.0776
7−	59.164204	2379.9	0.387	1.353	−0.6561	0.2309
7+	60.434778	2438.0	0.386	1.339	0.6342	−0.2825
9−	58.323877	2363.7	0.621	1.295	−0.1932	0.0436
9+	61.150562	2479.5	0.621	1.292	0.1014	−0.0584
11−	57.612486	2120.1	0.910	1.262	−0.5416	0.6056
11+	61.800158	2275.9	0.910	1.263	0.5014	−0.6619
13−	56.968211	1746.6	1.255	1.223	−0.3545	0.6451
13+	62.411220	1915.4	1.255	1.217	0.3029	−0.6759
15−	56.363399	1331.8	1.654	1.189	−0.2378	0.6547
15+	62.997984	1490.2	1.654	1.174	0.1856	−0.6675
17−	55.783815	945.3	2.109	1.134	−0.1172	0.6135
17+	63.568526	1078.0	2.108	1.134	0.0658	−0.6139
19−	55.221384	627.1	2.618	1.089	0.2560	0.2952
19+	64.127775	728.7	2.617	1.088	−0.3036	−0.2895
21−	54.671180	389.7	3.182	1.037	0.3558	0.2654
21+	64.678910	461.3	3.181	1.038	−0.3968	−0.2590
23−	54.130025	227.3	3.800	0.996	0.3170	0.3750
23+	65.224078	274.0	3.800	0.996	−0.3528	−0.3680
25−	53.595775	124.6	4.474	0.955	0.2227	0.5085
25+	65.764779	153.0	4.473	0.955	−0.2548	−0.5002
27−	53.066934	64.29	5.201	0.906	0.1349	0.6206
27+	66.302096	80.40	5.200	0.906	−0.1660	−0.6091
29−	52.542418	31.24	5.983	0.858	0.1388	0.6526
29+	66.836834	39.80	5.982	0.858	−0.1680	−0.6393
31−	52.021429	14.32	6.819	0.811	0.1667	0.6640
31+	67.369601	18.56	6.818	0.811	−0.1956	−0.6475
33−	51.503360	6.193	7.709	0.764	0.1947	0.6729
33+	67.900868	8.172	7.708	0.764	−0.2216	−0.6545
35−	50.987745	2.529	8.653	0.717	0.2246	0.680
35+	68.431006	3.397	8.652	0.717	−0.2492	−0.660
37−	50.474214	0.975	9.651	0.669	0.2566	0.685
37+	68.960312	1.334	9.650	0.669	−0.2773	−0.665
	368.498246	67.4	0.048	1.64	0	0
	424.763020	637.7	0.044	1.64[a]	0	0
	487.249273	237.4	0.049	1.60[a]	0	0
	715.392902	98.1	0.145	1.60	0	0
	773.839490	572.3	0.141	1.62[a]	0	0
	834.145546	183.1	0.145	1.47[a]	0	0

[a] Measured in previous works [9,11,12].

the center of the band, as seen in Fig. 12, where it contributes approximately ±1% to total absorption between 59 and 62 GHz. Microwave measurements from satellites or aircraft cannot observe this region of frequency and pressure due to the opacity of the atmosphere at higher altitudes, so a first-order model is quite adequate for those applications.

7. Conclusions

Improvement of microwave experimental technique and measurement methods achieved in [9–11] and in the present work, permitted accurate analysis of the 60-GHz oxygen absorption band, including detailed study of individual lines at pressures up to 4 Torr and measurement of the summed absorption profile in the range 45–96 GHz at atmospheric pressure and room temperature in laboratory air and pure oxygen. The most accurate to date values of central frequencies and self- and N_2-broadening parameters were obtained for the fine-structure oxygen lines up to $N = 27$. Precisely measured central frequencies allowed improvement of fine-structure spectroscopic constants for the oxygen molecule. The accurate measurement of broadening parameters allowed detailed analysis of their depen-

dence on rotational quantum number and the foreign-gas broadening efficiency. Comparison of our linewidth data with HITRAN and GEISA databases indicates that updating of these databases is necessary. Comparison of the fine-structure broadening data with corresponding data on the oxygen A-band reveals very similar dependence on the rotational quantum number N.

First-order mixing coefficients for the 60-GHz band in pure oxygen and in air were derived. Effects of second-order (in pressure) mixing were detected and showed similarity to theoretical predictions. The study revealed that at the present level of measurement accuracy the second order mixing effect cannot be neglected, and it was therefore treated as a source of error in the first-order model. We did not attempt to derive second-order mixing coefficients from the data. For that either an increase of experimental absorption profile signal-to-noise ratio by at least a factor of 10, or measurement of absorption profiles at higher pressures would be necessary.

The line parameters in MPM were updated with new intensities, widths, and mixing coefficients. This new model is expected to be more accurate at low pressures where the lines are resolved, while it provides similar results to MPM92 on the band wings.

The information obtained in course of this work can be applied to Earth atmosphere remote sensing, microwave wireless communication, and industrial applications (see e.g. [27]), as well as for fundamental spectroscopic studies.

In closing it should be mentioned that we plan to continue our study of the oxygen microwave spectrum in the direction of refinement of temperature dependences of line parameters, with the goal of further improvement of the MPM. Also, the problem of accurate derivation of both first- and second-order mixing coefficients could be addressed by developing a vacuum chamber for our resonator spectrometer. Then a more definite determination of first-order mixing coefficients could be achieved by having several absorption profile records in the pressure range from 100 Torr up to one atmosphere and above.

Acknowledgments

The authors are grateful to Professor A.F. Krupnov for his interest in this work and for stimulating discussions, to V.V. Parshin and S.E. Myasnikova for their help with the resonator spectrometer experiment, to A.F. Andrianov and A.P. Shkaev for their technical support, to S.E. Tretyakova for help with the paper artwork and to Agnes Perrin for her assistance in getting data from the most recent version of the GEISA databank. This work was supported in part by the Russian Fund for Basic Researches (Grant No. 03-02-16125) and by the Russian Ministry of Industry, Science and Technologies.

References

[1] P.W. Rosenkranz, IEEE Trans. Antenn. Prop. 23 (1975) 498–506.
[2] E.W. Smith, J. Chem. Phys. 74 (12) (1981) 6658–6673.
[3] J.H. Van Vleck, Astrophys. J. 80 (3) (1934) 161–170.
[4] R. Schlapp, Phys. Rev. 51 (1937) 342–345.
[5] R. Beringer, Phys. Rev. 70 (1 and 2) (1946) 53–57.
[6] J.H. Van Vleck, Phys. Rev. vol. 11 (7) (1947) 413–424.
[7] H.J. Liebe, Int. J. Infrared Mill. Waves 10 (1989) 631–650.
[8] H.J. Liebe, P.W. Rosenkranz, G.A. Hufford, J. Quant. Spectrosc. Radiat. Transfer 48 (5/6) (1992) 629–643.
[9] A.F. Krupnov, G.Yu. Golubiatnikov, V.N. Markov, D.A. Sergeev, J. Molec. Spectrosc. 215 (2002) 1–3.
[10] A.F. Krupnov, M.Yu. Tretyakov, V.V. Parshin, V.N. Shanin, S.E. Myasnikova, J. Molec. Spectrosc 202 (2000) 107–115.
[11] M.Yu. Tretyakov, G.Yu. Golubiatnikov, V.V. Parshin, M.A. Koshelev, S.E. Myasnikova, A.F. Krupnov, P.W. Rosenkranz, J. Molec. Spectrosc. 223 (2004) 31–38.
[12] G.Yu. Golubiatnikov, M.A. Koshelev, A.F. Krupnov, J. Molec. Spectrosc. 222 (2003) 191–197.
[13] G.Yu. Golubiatnikov, A.F. Krupnov, J. Molec. Spectrosc. 217 (2003) 282–287.
[14] G.Yu. Golubyatnikov, A.F. Krupnov, J. Molec. Spectrosc. 225 (2004) 222–224.
[15] H.J. Liebe, Radio Sci. 20 (5) (1985) 1069–1089.
[16] L.S. Rothman, A. Barbe, et al., J. Quant. Spectrosc. Radiat. Transfer 82 (1) (2003) 5–44, Available from: <http://cfa-www.harvard.edu/HITRAN>.
[17] N. Jacquinet-Husson, N.A. Scott, A. Chédin, A.A. Chursin, Atmos. Oceanic Opt. 16-3 (2003) 256–261, Available from: <http://ara.lmd.polytechnique.fr/geisa>.
[18] H.J. Liebe, G.A. Hufford, M.G. Cotton, AGARD Conf. Proc. 542 (1993) 3.1–3.10.
[19] H.J. Liebe, G.G. Gimmestad, J.D. Hopponen, IEEE Trans. Ant. Prop. AP-25 (3) (1977) 327–335.
[20] L.R. Brown, C. Plymate, J. Molec. Spectrosc. 199 (2000) 166–179.
[21] H.M. Pickett, J. Molec. Spectrosc. 148 (1991) 371–377, Available from: <http://spec.jpl.nasa.gov/> .
[22] M.Yu. Tretyakov, V.V. Parshin, M.A. Koshelev, V.N. Shanin, S.E. Myasnikova, A.F. Krupnov, J. Molec. Spectrosc. 218 (2003) 239–245.
[23] P.W. Rosenkranz, Radio Sci. 33 (1998) 919–928.
[24] Testo GmbH&Co. Available from: <http://www.testo.de>.
[25] R.R. Gamache, A. Goldman, L.S. Rothman, J. Quant. Spectrosc. Radiat. Transfer 59 (1998) 495–509.
[26] P.W. Rosenkranz, J. Quant. Spectrosc. Radiat. Transfer 39 (1988) 287–297.
[27] Y. Watanabe, T. Suzuki, T. Murakami, Y. Teshima, K. Shioda, P. Rosenkranz, in: Proc. URSI2002, F3.O.1, 2002.